Photoelectrochemical properties of dyads composed of porphyrin/ruthenium catalyst grafted on metal oxide semiconductors

Asterios Charisiadis, Eleni Glymenaki, Planchat Aurelien, Sofia Margiola, Anna-Caroline Lavergne-Bri, Emmanouil Nikoloudakis, Vasilis Nikolaou, Georgios Charalambidis, Athanassios G.Coutsolelos, Fabrice Odobel

Photoelectrochemical properties of dyads composed of porphyrin/ruthenium catalyst grafted on metal oxide semiconductors

Asterios Charisiadis,[a] Eleni Glymenaki,[a] Aurélien Planchat,[b] Sofia Margiola,[a] Anna-Caroline Lavergne,[a] Emmanouil Nikoloudakis,[a] Vasilis Nikolaou,[a] Georgios Charalambidis,[a] Athanassios G. Coutsolelos,[a] Fabrice Odobel.[b]**

[a]*Department of Chemistry, University of Crete, Laboratory of Bioinorganic Chemistry, Voutes Campus, Heraklion 70013, Crete, Greece. e-mail: acoutsol@uoc.gr*

[b]*Université LUNAM, Université de Nantes, CNRS, Chimie et Interdisciplinarité: Synthèse, Analyse, Modélisation (CEISAM), UMR 6230,2 rue de la Houssinière, 44322 Nantes cedex 3, France. e-mail: Fabrice.Odobel@univ-nantes.fr*

Abstract

In the current work, we present the use of two free-base and two zinc-metallated porphyrin-ruthenium(II) polypyridine dyads, along with two reference porphyrin derivatives, as sensitizers in both n- and p-type DSSCs and DSPECs. Two of the dyads contain the well-known $Ru(bpy)_3$ unit (**HOOC-DMP-Ru(bpy)$_3$** and **HOOC-(Zn)DMP-Ru(bpy)$_3$**), while in the other two terpyridine-Ru(Cl)-bypiridine was used (**HOOC-DMP-tpy-Ru** and **HOOC-(Zn)DMP-tpy-Ru**). In all systems, the amide-bonding motif was utilized for the connection of the counterparts comprising each dyad. Photophysical investigation of the reported systems indicated sufficient electronic interactions for the dyads in their excited states (emission measurements). The photovoltaic measurements revealed that the presence of the ruthenium complex improves the overall performance of the dyads with the most efficient dyad being **HOOC-(Zn)DMP-tpy-Ru** in both n- and p-type DSSCs. Consequently, **HOOC-(Zn)DMP-tpy-Ru** was used to fabricate n- and p-DSPECs towards the oxidation of methoxy-benzyl alcohol and the reduction of CO_2, respectively.

Introduction

Photoelectrochemical devices based on dye-sensitized wide bandgap semiconductors are the key components of photovoltaic devices, such as dye-sensitized solar cells (DSSCs),[1, 2] as well as artificial photosynthetic schemes, i.e.dye-sensitized photoelectrosynthetic cells (DSPECs)[3-6]. These integrated systems have attracted significant interest during the past decades since the properties they possess differ from those of each component. For example, TiO_2 and NiO are materials with low electrical conductivities; however, high photocurrent densities have been recorded upon their incorporation in DSSCs. Moreover, the frequently used **N3** dye [cis-bis(isothiocyanato)-bis(2,2'-bipyridyl-4,4'-dicarboxylato ruthenium(II)] exhibits poor photochemical stability. Though, once grafted on TiO_2, **N3** reaches outstanding lifetime values prior to its decomposition owing to very fast electron injection, which outcompetes with photodegradation processes.[7] DSSCs and DSPECs are also very appealing systems for solar energy conversion, since their operation principle closely mimics the procedures that take place in natural photosynthesis, achieving remarkable photoconversion efficiencies (PCEs), particularly in the case of TiO_2 based DSSCs.[8-11]

Porphyrins belong to the famous class of dyes that were successfully used as sensitizers in DSSCs both with TiO_2[8, 9, 12, 13] and NiO[14-20] semiconductors (SCs). The association of a ruthenium polypyridine complex with a porphyrin sensitizer is particularly appealing because the metal to ligand charge transfer transition (MLCT) of the Ru complex fills precisely the absorption gap of the porphyrin between the Soret and the Q-bands.[21, 22] Accordingly, the Ru complex could enhance the light harvesting ability of the porphyrin. Moreover, the ruthenium complex could be oxidized or reduced easier compared to the porphyrin ring serving as hole or electron acceptor, while diminishing the geminate charge recombination reaction. Finally, Meyer and co-workers, along with other groups, have demonstrated that tpy-Ru derivatives can work as catalysts for either alcohol oxidation[23-27] and/or for CO_2 reduction.[28-32] Consequently, the dyads containing the tpy-Ru unit could be implemented in DSPECs as photocatalysts for either alcohol oxidation on TiO_2 or CO_2 reduction on NiO. Alcohol oxidation seems to be more appealing than water oxidation into oxygen, because the latter requires four holes to operate instead of only two that are needed for alcohol oxidation and necessitates a higher potential (1.23 V *vs.* NHE for water *versus* -0.143 V *vs.* NHE for benzyl alcohol oxidation).[33] In other words, alcohol oxidation is a simpler reaction from both energetic and kinetic point of view. Moreover, oxygen has a little economic value while aldehydes are commodity chemical for the industry. DSPECs for alcohol oxidation were reported by Meyer and co-workers,[23, 24, 34] but these devices are much less investigated than the corresponding systems for water oxidation[3, 5, 6] in spite of their potentially greater interest. Interestingly, p-DSPECs based on NiO were also developed for CO_2 reduction,[35-38] but the performances are much poorer than those for oxidation with n-type semiconductors (SCs) because of the fast charge recombination process occurring on NiO sensitized devices.[2, 39, 40] To that end, we illustrate herein the thorough preparation of "porphyrin-ruthenium" dyads and their application in DSSCs and DSPECs examining their photoelectrochemical properties. In this study, two ruthenium complexes, namely the heteroleptic ruthenium terpyridine bipyridine (abbreviated tpy-Ru) or ruthenium tris-bipyridine (abbreviated $Ru(bpy)_3$) were linked to a porphyrin sensitizer in order to investigate whether the newly formed dyads would present improved overall performances in DSSCs or DSPECs (Chart).

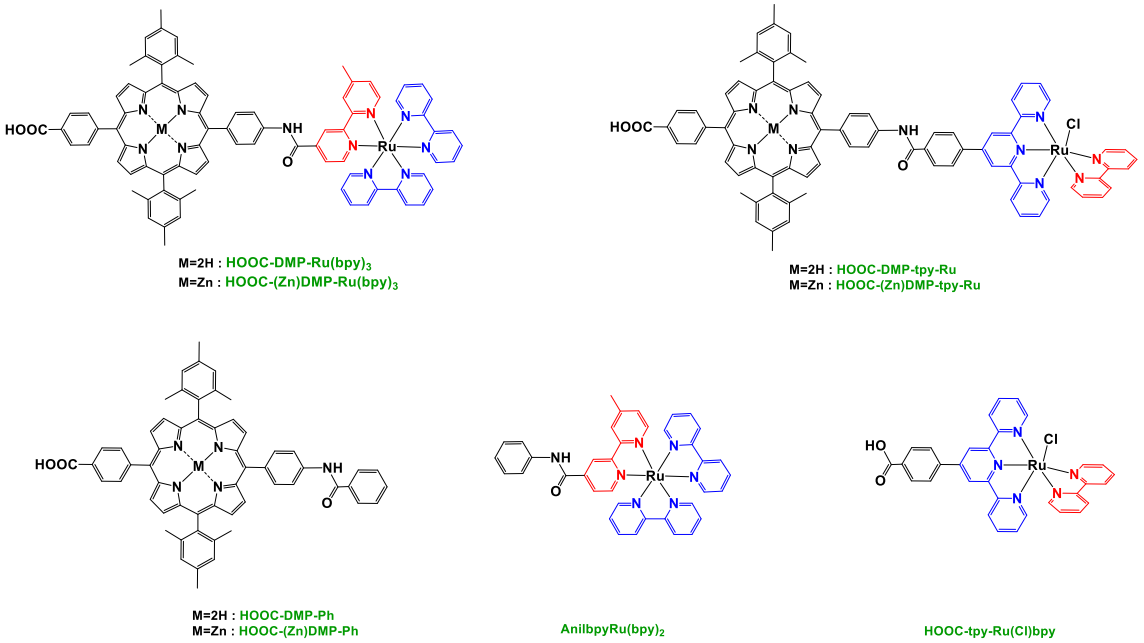

Chart 1. Structures of the compounds studied in this work.

All the results that derived from these two complementary devices, provided essential feedback in order to optimize and elucidate the most promising systems. Overall, dyad **HOOC-(Zn)DMP-tpy-Ru** was the most efficient complex due to the effective charge shift from the oxidized (or reduced) zinc porphyrin to the adjacent Ru complex, illustrating the higher light harvesting efficiency (LHE).

Results and discussion

Synthesis

All dyads consist of a porphyrin derivative coupled to a ruthenium(II) polypyridyl complex *via* an amide bond (Chart 1). In addition, in each porphyrin-ruthenium complex, carboxylic acid was introduced as anchoring group for the successful attachment of the dyad onto the surface of the semiconductor. Two of the dyads contain a free-base porphyrin while in the remaining two the macrocycle is metallated with zinc. The synthetic procedures that were followed for the preparation of all desired products are outlined in Schemes 1 and 2.

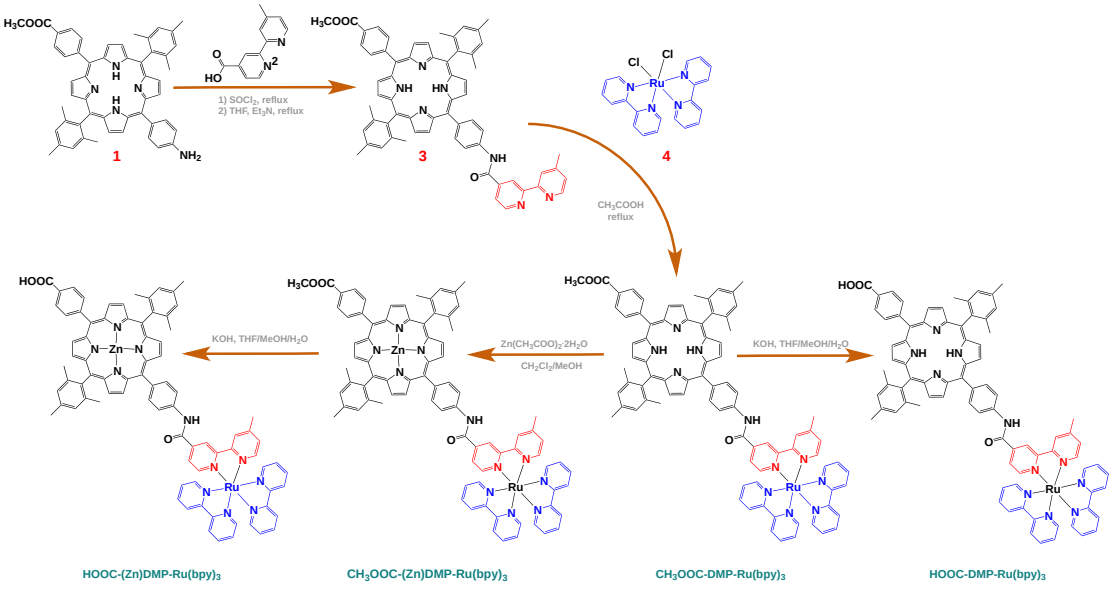

Scheme 1. Synthesis of dyads **HOOC-DMP-Ru(bpy)$_3$** and **HOOC-(Zn)DMP-Ru(bpy)$_3$**.

The synthesis of dyads **HOOC-DMP-Ru(bpy)$_3$** and **HOOC-(Zn)DMP-Ru(bpy)$_3$** is presented in Scheme 1. The porphyrin derivative **1**[41] was linked to carboxylic acid bipyridine compound (**2**)[42] *via* a two-step amide coupling reaction. More specifically, the carboxylic acid substituted bipyridine (**2**) was initially refluxed in $SOCl_2$ in order to obtain the corresponding acyl chloride, which then reacted with amino porphyrin (**1**) in the presence of Et_3N to afford the intermediate **3**. The next step involved the reaction of porphyrin **3** and ruthenium complex **4**[43] in acetic acid under reflux. Subsequently, the free base dyad **CH$_3$OOC-DMP-Ru(bpy)$_3$** underwent a basic hydrolysis reaction forming the desired dyad **HOOC-DMP-Ru(bpy)$_3$**. Regarding the metallated dyad, **CH$_3$OOC-DMP-Ru(bpy)$_3$** was treated with an excess of zinc acetate in a CH_2Cl_2/MeOH mixture leading to the formation of dyad **CH$_3$OOC-(Zn)DMP-Ru(bpy)$_3$**. Finally, through a basic hydrolysis reaction, **HOOC-(Zn)DMP-Ru(bpy)$_3$** was afforded that contains the desired carboxylic acid anchoring group.

The synthesis of the terpyridine-based dyads (**HOOC-DMP-tpy-Ru** and **HOOC-(Zn)DMP-tpy-Ru**) as well as the two porphyrin reference compounds (**HOOC-DMP-Ph** and **HOOC-(Zn)DMP-Ph**) is shown in Scheme 2. All the methyl-ester derivatives (**CH$_3$OOC-DMP-tpy-Ru**, **CH$_3$OOC-**

(Zn)DMP-tpy-Ru, **CH_3OOC-DMP-Ph** and **CH_3OOC-(Zn)DMP-Ph**) have been prepared according to procedures previously reported by our group.[44]

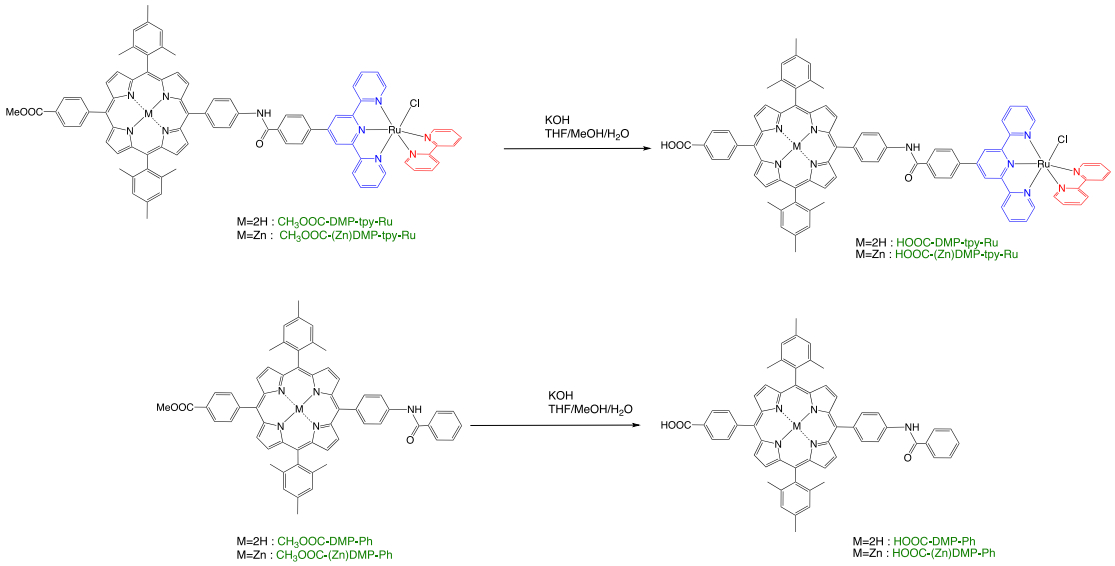

Scheme 2. Preparation of dyads **HOOC-DMP-tpy-Ru** and **HOOC-(Zn)DMP-tpy-Ru** as well as the two reference compounds (**HOOC-DMP-Ph** and **HOOC-(Zn)DMP-Ph**).

The four final compounds (**HOOC-DMP-tpy-Ru**, **HOOC-(Zn)DMP-tpy-Ru**, **HOOC-DMP-Ph** and **HOOC-(Zn)DMP-Ph**) were prepared through the hydrolysis of the methyl ester groups to the desired carboxylic acid anchoring groups. All intermediates and final products were fully characterized by ^{1}H and ^{13}C NMR spectroscopy (Figures S1-S30) and MALDI-TOF mass spectrometry.

Photophysical Properties

Figures 1 and 2 present the electronic absorption spectra of the reference compounds as well as the porphyrin-ruthenium dyads. The absorption spectrum of the free-base reference derivative (**HOOC-DMP-Ph**, Figure S31) in THF exhibits typical porphyrin absorption features with an intense Soret band at 419 nm and four Q bands of moderate intensity (516, 549, 593, and 650 nm). These features are also present in the absorption spectrum of the **HOOC-DMP-Ru(bpy)$_3$** dyad in a THF/MeOH (1:1) mixture (Figure S32), accompanied by two additional bands at 292 and approximately 460 nm (shoulder) that are attributed to the $^{1}\pi$-π^{*} transition and the MLCT of the Ru(bpy)$_3$ unit, respectively.[43, 45] Furthermore, the spectrum of **HOOC-DMP-tpy-Ru** in THF (Figure S33) exhibits absorption peaks that correspond to the porphyrin moiety as well as some characteristic bands of the tpy-Ru part.[44] In particular, three peaks can be detected at 292, 323 and 515 nm, which are attributed to the LC, MC and MLCT bands, respectively. As expected, in the case of the metallated reference derivative (**HOOC-(Zn)DMP-Ph**, Figure S34), typical porphyrin absorption features were observed. More specifically, the Soret band (426 nm) was slightly shifted and the number of the Q bands (557 and 598 nm) was reduced compared to **HOOC-DMP-Ph**, due to the increased symmetry of this compound. Moreover, these features are also displayed in the UV-Vis spectra of both Zn-metallated dyads accompanied by the characteristic bands of each corresponding Ru-based unit (Figures S35 and S36). Taking into account these observations, it is clear that the individual spectroscopic

features of the two moieties are not significantly altered in the dyads. Therefore, the UV-Vis absorption spectra of the four dyads can be described as the sum of the spectra of their constituent chromophores, suggesting that in all cases the two moieties interact only weakly in the ground state.

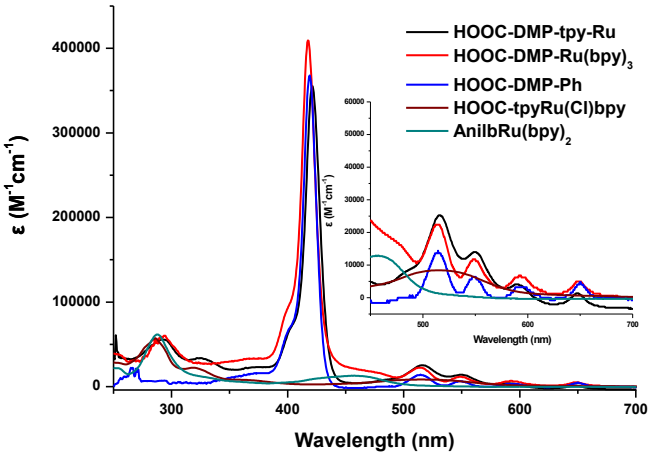

Figure 1. UV-vis absorption spectra of the free-base dyads (**HOOC-DMP-Ru(bpy)$_3$** in THF/MeOH and **HOOC-DMP-tpy-Ru** in THF) and the reference compounds **HOOC-DMP-Ph** in THF, **HOOC-tpyRu(Cl)bpy** and **AnilbpyRu(bpy)$_2$** in CH_3CN.

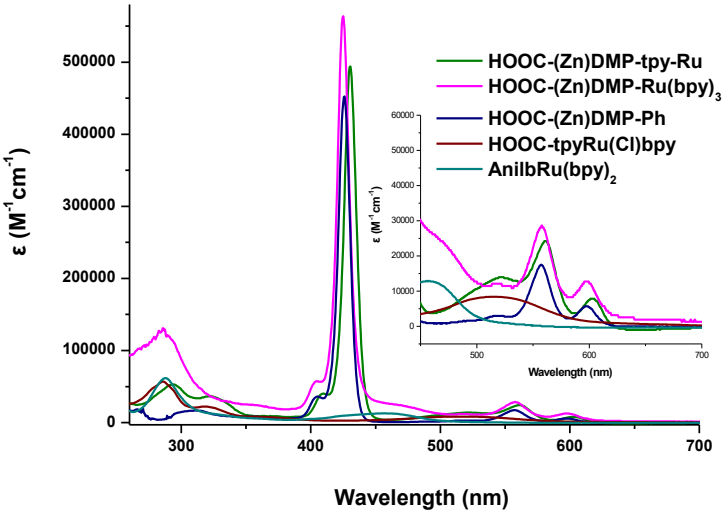

Figure 2. UV-vis absorption spectra of the metallated dyads (**HOOC-(Zn)DMP-Ru(bpy)$_3$** in THF/MeOH and **HOOC-(Zn)DMP-tpy-Ru** in THF) and the reference compound **HOOC-(Zn)DMP-Ph** in THF, **HOOC-tpyRu(Cl)bpy** and **AnilbpyRu(bpy)$_2$** in CH_3CN.

Initial insights into the possible donor-acceptor interactions between the porphyrin and the ruthenium moieties, were obtained from fluorescence spectroscopy studies. The emission spectra of the dyads were recorded in THF/MeOH solutions, upon excitation at 550 nm, and compared with the corresponding spectra of the reference porphyrin compounds (Figures S37 and S38). Both reference compounds (**HOOC-DMP-Ph** and **HOOC-(Zn)DMP-Ph**) demonstrated strong emissions in the 520-750 nm range, with two maxima at 655 and 718 nm and at 607 and 656 nm, respectively. The spectra of the dyads displayed practically identical shapes to those obtained for their reference derivatives with insignificant contribution from the ruthenium chromophore. However, in all cases the porphyrin fluorescence was significantly quenched. The emission intensity of the three dyads (**HOOC-(Zn)DMP-Ru(bpy)$_3$**, **HOOC-DMP-tpy-Ru** and **HOOC-(Zn)DMP-tpy-Ru**) was considerably reduced (92%, 96% and 99%, respectively), while in the **HOOC-DMP-Ru(bpy)$_3$** dyad, the emission intensity was slightly quenched (29%) compared to the **HOOC-DMP-Ph**. These observations suggest the presence of an intramolecular decay channel, which most probably originates from an energy transfer reactions from the singlet excited state of the porphyrin to the triplet MLCT of Ru complex which is followed by a triplet to triplet energy transfer to finally form the porphyrin triplet excited state in all the dyads**.** This behavior have been previously demonstrated by photophysical studies in solution of the compounds and **HOOC-DMP-tpy-Ru** and **HOOC-(Zn)DMP-tpy-Ru** and on dyads closely related to **HOOC-DMP-Ru(bpy)$_3$** and **HOOC-(Zn)DMP-Ru(bpy)$_3$**.

Electrochemical Characterization

The electrochemical features of all dyads as well as their reference compounds were examined using cyclic (CV) and square wave (SW) voltammetry in benzonitrile solutions containing 0.1M tetrabutylammonium hexafluorophosphate (Bu_4NPF_6) as the supporting electrolyte. The redox potentials are summarized in Table 1, while the voltammograms are presented in Figures S39-S41.

Table 1. Electrochemical data recorded in benzonitrile solutions containing 0.1M Bu_4NPF_6 as the supporting electrolyte and FcH/FcH^+ as internal standard.[a]

	E_{red2} (P)	E_{red3} (Rubpy)	E_{red2} (Rutpy)	E_{red2} (Rubpy)	E_{red1} (Rutpy)	E_{red1} (P)	E_{red1} (Rubpy)	E_{ox1} (Rutpy)	E_{ox1} (P)	E_{ox2} (P)	E_{ox1} (Rubpy)
CH_3OOC-DMP-Ph[b]	-1.58	-	-	-	-	-1.08	-	-	1.14	1.42	-
CH_3OOC-(Zn)DMP-Ph[b]	-	-	-	-	-	-1.25	-	-	0.90	1.25	-
AnilbpyRu(bpy)$_2$	-	-1.53	-	-1.34	-	-	-1.09	-	-	-	1.47
CH_3OOC-DMP-Ru(bpy)$_3$	-1.53	-1.53	-	-1.36	-	-1.09	-1.09	-	1.14	1.47	1.47
CH_3OOC-(Zn)DMP-Ru(bpy)$_3$	-	-1.51	-	-1.30	-	-1.30	-1.11	-	0.89	1.21	1.47
HOOC-tpyRu(Cl)bpy[b]	-	-	-1.42	-	-1.25	-	-	0.94	-	-	-
CH_3OOC-DMP-tpy-Ru[b]	-1.58	-	-1.42	-	-1.23	-1.09	-	0.93	1.13	1.37	-
CH_3OOC-(Zn)DMP-tpy-Ru[b]	-	-	-1.41	-	-1.25	-1.25	-	0.93	0.93	1.22	-

[a]All potentials are in V *vs.* SCE. [b]From ref. [17].

Owing to the weak ground state electronic interactions between the two chromophores, the observed redox processes in the dyads can confidently be assigned by comparing the respective potentials of the corresponding reference compounds. For example, in **CH_3OOC-(Zn)DMP-Ru(bpy)$_3$** the observed electrochemical waves correspond to those obtained separately for its constitutive units **CH_3OOC-(Zn)DMP-Ph** and **AnilbpyRu(bpy)$_2$**. Three oxidation waves were detected with the first two (0.89 V and 1.21 V) being assigned to the porphyrin macrocycle, while the potential located at 1.47 V *vs.* SCE was attributed to the oxidation of ruthenium unit. On the cathodic side, peaks at -1.11 V and -1.51 V originate from the reduction of the ligands on Ru(bpy)$_3$ moiety (formally written Ru(I) although it is a ligand centered process). The wave at -1.30 V corresponds to the simultaneous reduction of the porphyrin and the ruthenium complex. All the above results suggest that the covalent linkage between the two constituent chromophores (porphyrin and ruthenium dye) had little effect in the redox potentials of the dyads. Interestingly, the porphyrin macrocycle is more easily oxidized in the **CH_3OOC-(Zn)DMP-Ru(bpy)$_3$** dyad while the first reductive wave corresponds to the Ru(bpy)$_3$ part. As far as the **CH_3OOC-DMP-Rutpy** and **CH_3OOC-(Zn)DMP-Rutpy** dyads are concerned, the oxidation of the ruthenium complex is close to that of the porphyrin indicating that hole shift reaction (reaction 3) has an almost insignificant driving force. Likewise, the reduction of the zinc porphyrin is very similar to that of the Ru complex indicating that electron shift reaction (reaction 4) is poorly exergonic, while it is clearly endergonic with the free base porphyrin in **CH_3OOC-DMP-Rutpy** (Scheme 5). It is important to point out that the redox potential of the Rutpy moiety is likely to change in DSSC and DSPEC, because the chloro ligand will possibly be exchanged with water or acetonitrile molecules. For example, it was reported that the replacement of a chloro by an aquo ligand in the Ru complex RubpytpyCl induces a *circa* 300 mV cathodic shift of the oxidation potential of the Ru center.[27]

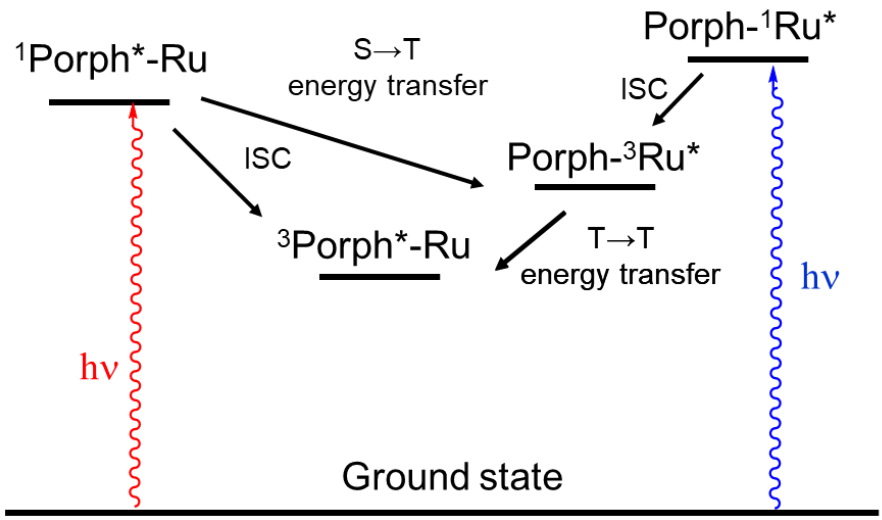

Scheme 3. Relative position of the energy levels of excited states of the components of the dyads and summary of the potential deactivation processes occurring in solution upon excitation of the porphyrin (red arrow) or the ruthenium complex (blue arrow).

The redox potentials along with the energy level of the porphyrin excited state now enable us to determine the Gibbs free energy of the potential electron transfer processes in the dyads

and with the TiO_2 and NiO semiconductors and the data are collected in Table 2. The charge transfer processes that take place are, firstly, the electron injection in the TiO_2 conduction band (reaction 1) and, secondly, the hole injection in NiO valence band (reaction 2) from the porphyrin excited state (Porph*).

Porph*-TiO_2 → $^{+}$Porph-TiO_2(e-) reaction 1 ($\Delta G_{e\text{-}inj}$)

Porph*-NiO → $^{-}$Porph-NiO(h^{+}) reaction 2 (ΔG_{h+inj})

The formation of the triplet excited state of the porphyrin sensitizers is very likely to occur in these dyads, owing to intersystem crossing (ISC) promoted by the nearby ruthenium complex or triplet-triplet (T→T) energy transfer from the MLCT of the appended ruthenium complex to the porphyrin (Scheme 3).[44, 46, 47] The Gibbs free energies of the electron injection in TiO_2 ($\Delta G_{e\text{-}inj}$) and the hole injection in NiO (ΔG_{h+inj}) were calculated from both the singlet and the triplet excited states of the porphyrins (Table 2).

Table 2. Values of the Gibbs free energy of the electron transfer processes in the compounds.

Compounds	$^{1}\Delta G_{e\text{-}inj}$ **(eV)**[a]	$^{3}\Delta G_{e\text{-}inj}$ **(eV)** [b]	$^{1}\Delta G_{h+inj}$ **(eV)**[a]	$^{3}\Delta G_{h+inj}$ **(eV)**[b]	ΔG_{h+s} **(eV)**[c]	$\Delta G_{e\text{-}s}$ **(eV)**[d]
HOOC-DMP-Ph	-0.07	+0.33	-0.53	-0.13	-	-
HOOC-DMP-Ru(bpy)$_3$	-0.07	+0.33	-0.52	-0.12	+0.33	0.0
HOOC-DMP-tpy-Ru	-0.08	+0.32	-0.52	-0.12	-0.20	+0.14
HOOC-(Zn)DMP-Ph	-0.46	+0.01	-0.51	-0.04	-	-
HOOC-(Zn)DMP-Ru(bpy)$_3$	-0.47	0.0	-0.46	+0.01	+0.58	-0.19
HOOC-(Zn)DMP-tpy-Ru	-0.43	+0.04	-0.51	-0.04	0	0.0

[a]charge injection from the singlet excited state of the porphyrin (^{1}Porph*). $E_{00}(^{1}ZnP^{*})$ = 2.06 eV; $E_{00}(^{1}P2H^{*})$ = 1.91 eV, measured with the intersection of the normalized absorption and emission spectra of the reference compounds; $^{1}\Delta G_{e\text{-}inj} = E_{Ox}(Porph^{+}/Porph) - E_{00}(^{1}Porph^{*}) + E_{CB}(TiO_2)$; $^{1}\Delta G_{h+inj} = E_{VB}(NiO) - E_{Red}(Porph/Porph^{-}) - E_{00}(^{1}Porph^{*})$ with $E_{CB}(TiO_2)$= -0.7 V *vs.* SCE and $E_{VB}(NiO)$= 0.3 V *vs.* SCE. [b]charge injection from the triplet excited state of the porphyrin (^{3}Porph*). $E_{00}(^{3}ZnP)$ = 1.59 eV; $E_{00}(^{3}P2H)$ = 1.51 eV taken from ref.[44]. $^{3}\Delta G_{e\text{-}inj} = E_{Ox}(Porph^{+}/Porph) - E_{00}(^{3}Porph^{*}) + E_{CB}(TiO_2)$; $^{1}\Delta G_{h+inj} = E_{VB}(NiO) - E_{Red}(Porph/Porph^{-}) - E_{00}(^{3}Porph^{*})$.[c]hole shift reaction calculated from: $\Delta G_{h+s} = E_{Ox}(Ru(III)/Ru(II)) - E_{Ox}(Porph^{+}/Porph)$.[d]electron shift reaction calculated from: $\Delta G_{e\text{-}s} = E_{Red}(Porph/Porph^{-}) - E_{Red}(Ru(II)/Ru(I))$.

The Gibbs free energies that were calculated for the charge transfer processes between the porphyrin and the SC indicate that: 1) electron injection in TiO_2 is a favorable reaction from zinc porphyrin singlet excited state, but the driving force is almost insignificant from the triplet excited state. However, it is possible to take place when a large concentration of lithium cation is used due to band bending[48, 49]. 2) Electron injection from the free base porphyrin to the TiO_2 is not only a poorly favorable reaction already from the singlet excited state but also very endergonic from the triplet, meaning that it is very unlikely to occur in the latter case. 3) Hole

injection in NiO is exergonic with the free base porphyrin from both singlet and triplet excited states. 4) Regarding the zinc porphyrin derivatives,, the driving force is significant (-0.5 eV) from the singlet excited state, but weak from the triplet excited state.

Secondly, the two important charge transfer reactions are: i) the hole shift from the oxidized porphyrin to the ruthenium complex (reaction 3) after electron injection into TiO_2 and ii) the electron shift (reaction 4) from the reduced porphyrin to the ruthenium complex after hole injection into NiO.

$Ru(II)/^{+}Porph\text{-}TiO_2(e\text{-}) \rightarrow Ru(III)/Porph\text{-}TiO_2(e\text{-})$ reaction 3 (ΔG_{h+s})

$Ru(II)/^{-}Porph\text{-}NiO(h^{+}) \rightarrow Ru(I)/Porph\text{-}NiO(h^{+})$ reaction 4 (ΔG_{e-s})

The calculated Gibbs free energies of these two reactions indicate that: 1) the hole shift reaction to oxidize the Rutpy catalyst is favorable only in the case of free base porphyrin entities. However, in water the chloro ligand on ruthenium is substituted by aqua and the oxidation of the ruthenium is cathodically shifted by 0.3 eV,[27] suggesting that this reaction is certainly exergonic in aqueous electrolyte with both dyads (**HOOC-DMP-tpy-Ru** and **HOOC-(Zn)DMP-tpy-Ru**). 2) Electron shift reaction from the radical anion of the porphyrin to the Rutpy catalyst (reaction 4) has no driving force regarding free base porphyrin, but becomes significantly allowed concerning the zinc metallated analogue in **HOOC-(Zn)DMP-tpy-Ru**.

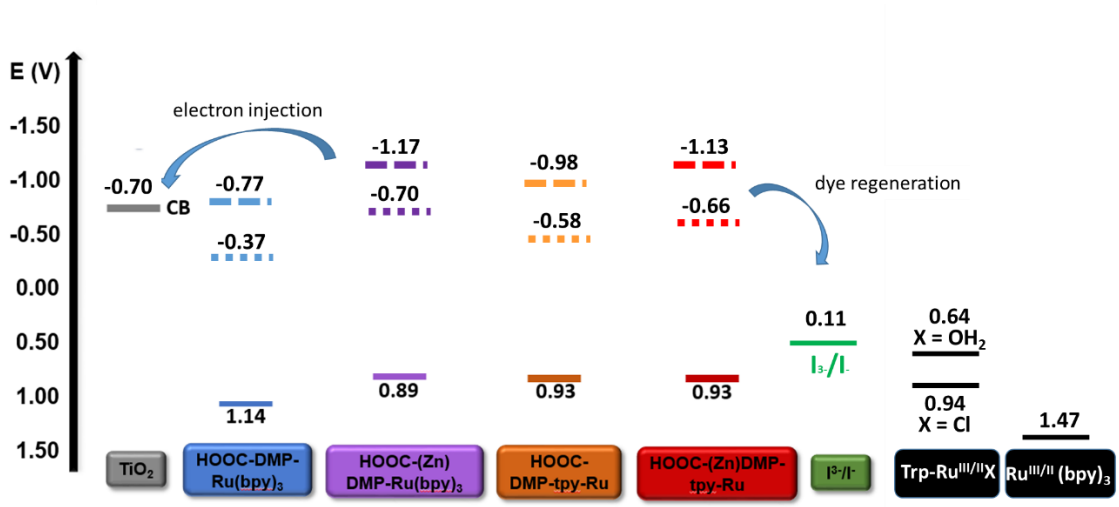

Scheme 4. Diagram showing the oxidation potential of the porphyrin sensitizer from the ground state (straight line), singlet excited state (dashed line), triplet excited state (dotted line), the reduction potential of the Ru complexes, the redox potential of the iodide based mediator and the potential of the TiO_2 conduction band (CB).

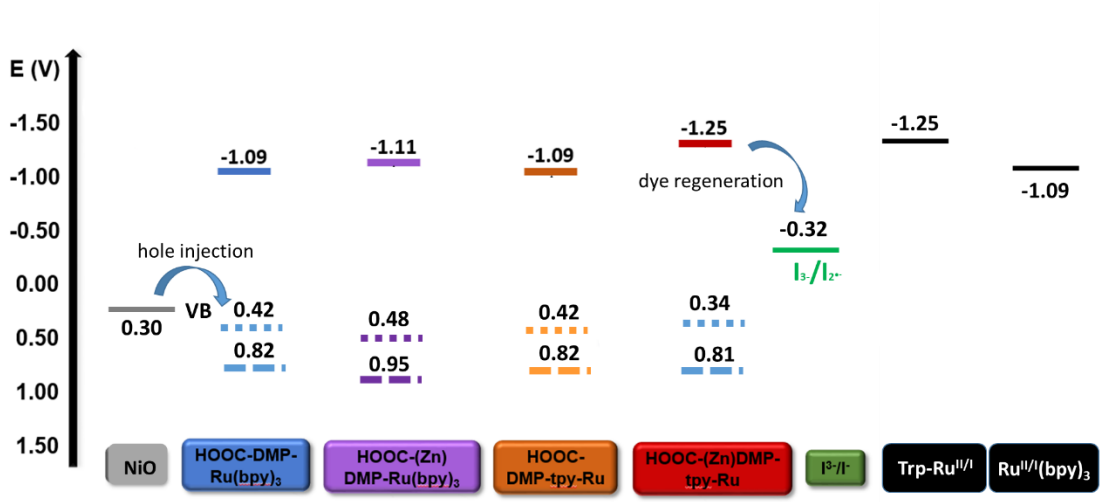

Scheme 5. Diagram showing the reduction potential of the porphyrin sensitizer from the ground state (straight line), the singlet excited state (dashed line), triplet excited state (dotted line), the reduction potential of the Ru complex, the redox potential of the iodide based mediator and the potential of the NiO valence band (VB).

Photovoltaic measurements in TiO_2 based n-DSSCs

All the compounds were used as sensitizers in DSSCs with TiO_2 photoanodes and using iodide/triiodide redox mediator (see experimental part for details). First, the chemisorption conditions were optimized by screening the dyeing bath composition and the soaking time with the dyad **HOOC-(Zn)DMP-tpy-Ru**. Two mixtures of solvents (THF/MeOH : 1/1 and Toluene/EtOH : 1/1) and three dyeing durations (2h, 4h and 8h) were investigated and it was found that the mixture Toluene/EtOH: 1/1 for 2 hours of soaking at room temperature gives the maximum power conversion efficiency (Table S1). These conditions were subsequently used for the fabrication of all the cells in this study. The average metrics of several solar cells are listed in Table 3 and the current/voltage characteristics are gathered in Figures S42-43 in ESI. The photoaction spectra are shown in Figure 3 except that of **HOOC-DMP-tpy-Ru**, which could not be recorded due to the too low photocurrent density delivered by the cell.

Table 3. Average metrics of solar cells measured under simulated AM1.5 (1000W/m^2).

Compounds	J_{SC} (mA/cm^2)	V_{oc} (mV)	ff (%)	PCE (%)
HOOC-DMP-Ph	1.08 ± 0.1	276 ± 1	64.4 ±0.3	0.19 ±0.02
HOOC-DMP-Ru(bpy)$_3$	0.60 ± 0.1	260 ± 3	63.3 ±0.8	0.10 ±0.01
HOOC-DMP-tpy-Ru	0.28 ± 0.2	263 ± 7	61.6 ±0.2	0.04 ±0.01
HOOC-(Zn)DMP-Ph	4.54 ± 0.2	340 ± 10	67.4 ±0.5	1.03 ±0.07
HOOC-(Zn)DMP-Ru(bpy)$_3$	3.60 ± 0.3	329 ± 2	65.6 ±0.1	0.77 ±0.05
HOOC-(Zn)DMP-tpy-Ru	4.21 ± 0.3	359 ± 2	67.1 ±0.2	1.01 ±0.06

Zinc porphyrin derivatives are more efficient sensitizers than the corresponding free base porphyrins, predominantly due to a higher short circuit current density.[50] This can be attributed to the higher electron injection driving force for the zinc porphyrin systems (Table 2, Scheme 4). Indeed, the Gibbs free energy of the injection reaction from the free base

porphyrin's singlet excited state is almost absent and it even becomes positive from the triplet excited state. Secondly, for all the dyads, the efficiencies of the solar cells were lower in comparison with the reference sensitizers **HOOC-DMP-Ph** or **HOOC-(Zn)DMP-Ph**. This indicates that the presence of a ruthenium complex deactivates the porphyrin excited state through a process, which is competitive to the electron injection reaction (Scheme 4). Referring to the photophysical study of the dyads **HOOC-DMP-tpy-Ru** and **HOOC-(Zn)DMP-tpy-Ru** in solution,[44] we can reasonably conclude that the singlet excited state of the porphyrin is quenched by a singlet to triplet (S→T) energy transfer process to initially generate the triplet MLCT on the Ru complex. The triplet excited Ru complex subsequently decays according to a triplet to triplet (T→T) energy transfer process leading to the triplet excited state of the porphyrin, since it is the lowest lying excited state of the dyads (Scheme 3). The latter cannot efficiently promotes an electron injection to TiO_2 because the Gibbs free energy is too feeble and even positive for the free base porphyrin dyads (Scheme 4). Interestingly, this detrimental S→T energy transfer process seems to be less important with the tpy-Ru than with the $Ru(bpy)_3$ complex, most probably due to the longer distance between the porphyrin and the Ru center.

We can also note that the PCE of **HOOC-(Zn)DMP-tpy-Ru** and the reference sensitizer **HOOC-(Zn)DMP-Ph** is, within experimental errors, quite similar. The fairly lower J_{SC} counterbalances the slightly higher V_{OC}. On one hand, the higher V_{OC} value suggests that the hole shift reaction from ZnP^+ to Ru(II) (reaction 3) is probably favorable in this dyad. It is well accepted that as the hole shifts further from the semiconductor surface in **HOOC-(Zn)DMP-tpy-Ru**, the charge recombination process becomes slower leading to higher V_{OC}.[51] On the other hand, the lower J_{SC} can probably be attributed to the detected quench of the excited state of the porphyrin by the Ru complex according to a S→T energy transfer process. Indeed, the IPCE spectrum of the dyad displays lower IPCE values on the porphyrin absorption bands, namely the Soret (around 420 nm) and the Q-bands (550 and 600 nm) due to a competing energy transfer. Nonetheless, these current losses are compensated by the antenna effect of the MLCT absorption of the Ru complex (around 450 nm) clearly visible by the superior IPCE of **HOOC-(Zn)DMP-tpy-Ru** compared to that of **HOOC-(Zn)DMP-Ph** in this region (Figure 3). One possible strategy to enhance the quantum yield of the electron injection reaction over the S→T energy wasting process would be to increase the electronic coupling of the porphyrin with TiO_2 by introducing a triple bond between the benzoic acid anchoring unit and the porphyrin to increase the electron injection rate constant. Another possible way of decreasing the energy transfer rate constant, while retaining an efficient hole shift process (reaction 3), is by further elongating the distance between the Ru complex and the porphyrin. The rate of the latter process can be decreased, because the lifetime of the radical cation sensitizer is usually long on TiO_2.

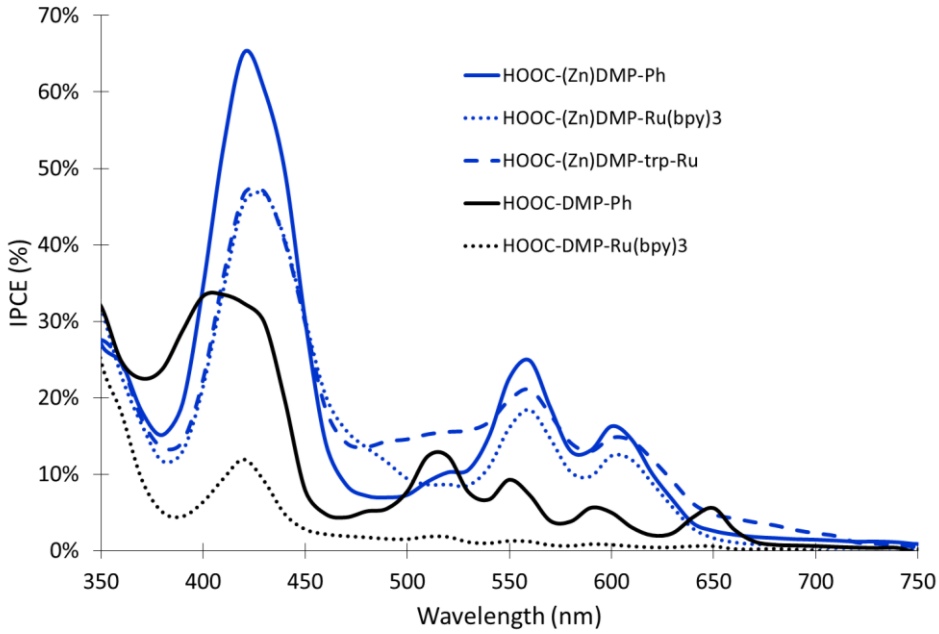

Figure 3. Photoaction spectra of the sensitizers in TiO_2 based DSSCs. The back curves correspond to free base porphyrin derivatives, while the blue ones to zinc porphyrin derivatives.

The comparison of the $Ru(bpy)_3$ *versus* tpy-Ru indicates that $Ru(bpy)_3$ has a more negative impact on the PV performances probably because the hole shift reaction is thermodynamically forbidden for $Ru(bpy)_3$, due to the fact that it is more difficult to oxidize than tpy-Ru. Besides, its higher proximity to the porphyrin induces a more efficient quenching by energy transfer.

Overall, based on the PV measurements in TiO_2 based DSSCs, it is clear that the most interesting dyad within these series is **HOOC-(Zn)DMP-tpy-Ru**, since it displays the highest efficiency. More importantly, the results of **HOOC-(Zn)DMP-tpy-Ru** illustrate that the presence of Ru moiety is beneficial due to an antenna effect (*via* the MLCT absorption band) and the occurrence of the hole shift reaction from ZnP^+ to Ru(II).

Photovoltaic measurements in NiO based p-DSSCs

The photovoltaic properties of these new compounds were also investigated in NiO based p-DSSCs with iodide/triiodide redox mediator using the optimized dyeing conditions that were determined for the TiO_2 based cells (see experimental part for details). The average metrics of several solar cells are gathered in Table 4 and the current/voltage characteristics are gathered in Figures S44-45 in ESI. The photoaction spectra are shown in Figure 4.

Table 4. Average metrics of solar cells measured under simulated AM1.5 (1000W/m^2).

Compounds	J_{SC} (mA/cm^2)	V_{OC} (mV)	ff (%)	PCE (%)
HOOC-DMP-Ph	0.79± 0.08	47 ± 2	30 ± 1	0.011 ± 0.01
HOOC-DMP-Ru(bpy)$_3$	0.89± 0.02	49 ± 5	30 ± 1	0.013 ± 0.02
HOOC-DMP-tpy-Ru	0.96± 0.06	59 ± 2	32 ± 1	0.018 ± 0.01
HOOC-(Zn)DMP-Ph	0.96 ± 0.08	70 ± 6	33 ± 1	0.018 ± 0.01

HOOC-(Zn)DMP-Ru(bpy)$_3$	1.10 ± 0.02	80 ± 2	34 ± 1	0.030 ± 0.01
HOOC-(Zn)DMP-tpy-Ru	1.26 ± 0.03	93 ± 1	30 ± 1	0.035 ± 0.01

Similarly to the n-type solar cells, the zinc porphyrin is the more efficient sensitizer compared to the free base derivative. However, the interpretation of this result is not obvious at this stage, because the hole injection driving force is similar for both compounds and the geminate charge recombination, which is particularly acute on NiO based p-DSSCs,[2, 39] should not be so different in both dyes as the radical anion is localized on the aromatic ring of the porphyrin macrocycle. Very interestingly and contrary to the photovoltaic results on TiO_2, the dyads with the appended Ru complex display higher efficiencies in NiO based p-DSSCs than the reference porphyrins particularly due to higher J_{SC} and V_{OC} (Table 4). Interestingly, connecting a tpy-Ru unit to the porphyrin sensitizer significantly improves the performances of these dyads (**HOOC-DMP-tpy-Ru** and **HOOC-(Zn)DMP-tpy-Ru**). Moreover, the V_{OC} values are higher for the dyads compared to the reference derivatives, suggesting that the charge recombination is lower, because NiO based DSSCs are particularly prone to this deleterious energy wasting process.[2, 39] The occurrence of the electron shift reaction from the reduced porphyrin to the Ru complex (reaction 4) is not highly favorable as calculated with the chloro ligand (Table 2). However, in the electrolyte ligand scrambling from chloro to acetonitrile around Ru center is highly likely to take place, therefore the reduction potential of the complex is probably less negative, because acetonitrile is a less electron donating than chloro. This is consistent with the work of Ott and coll. (ref. 31) who showed that the reduction potential of a Ru(tpy)(Me_2bpy)X is anodically shifted by about 160 mV when chloro ligand is replaced by acetonitrile. Accordingly, the feasibility of the electron shift can be excluded only in the case of the dyad **HOOC-DMP-Ru(bpy)$_3$**, which consistently displays, within experimental error, a similar Voc as the reference **HOOC-DMP-Ph**. However, we cannot excluded another reason for the higher Voc and it is possible that ruthenium complex, being a positively charged compound, makes ion pairing with triiodide anion increasing thus the regeneration rate and consequently diminishes charge recombination. Similar phenomenon has been reported in TiO_2 based DSSCs by Meyer and coll. (ref. X) On the other hand, the higher J_{SC} in the dyads can be ascribed to their higher light harvesting efficiency as confirmed by the significantly higher IPCE around 500 nm. This can be understood as the result of either an energy transfer from the Ru chromophore to the porphyrin, either a direct hole injection from the MLCT of the Ru complex or the lower charge recombination due to the longer distance between the NiO surface and the oligopyridine ligand of the Ru complex.

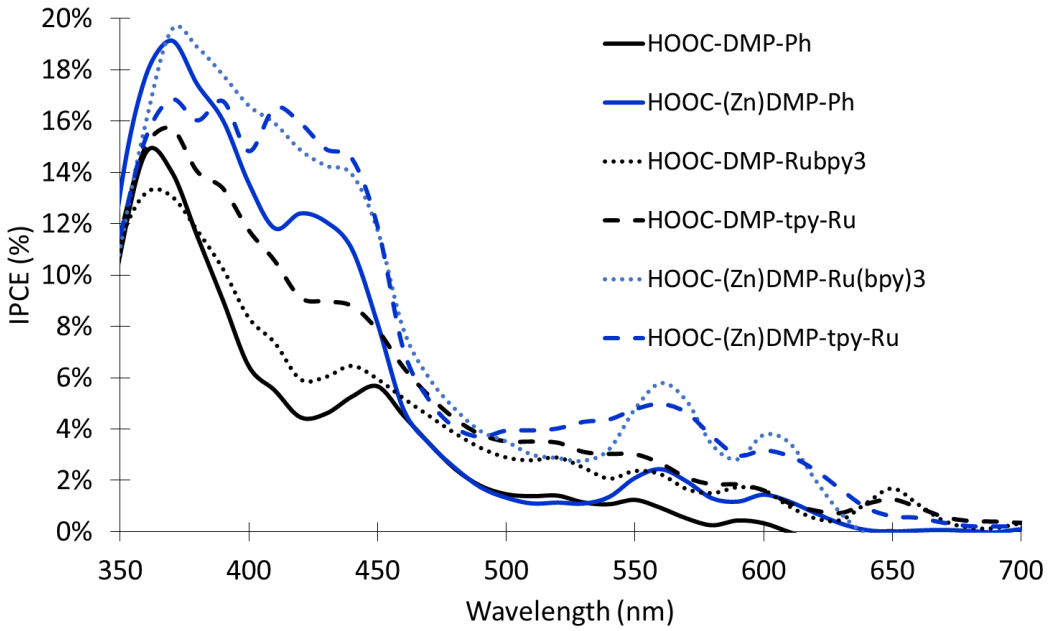

Figure 4. Photoaction spectra of the sensitizers in NiO based p-DSSC. The back curves correspond to free base porphyrin derivatives while the blue ones to zinc porphyrin derivatives.

In conclusion, the introduction of a ruthenium complex to the zinc porphyrin slightly enhances the photovoltaic efficiency on NiO based p-DSSCs and the dyad **HOOC-(Zn)DMP-tpy-Ru** is certainly the most attractive system in the series as it gives the highest performances and it is potentially useful for photocatalysis in DSPECs.

Photocatalytic tests

Initially, we investigated the ability of **HOOC-(Zn)DMP-tpy-Ru** to oxidize *para* methoxy benzyl alcohol into the corresponding aldehyde, upon the attachment of the dyad onto a TiO_2 electrode in an acetate buffer (pH = 4.75). Other conditions such as buffer/organic solvent mixtures (acetate buffer/CH_3CN (or acetone): 1/1 and 7/3) and at other pH (4, 5 and 7.5) were tested but the photocurrent was not highest than in pure acetate buffer at pH 4.75 in agreement with another study. In this study, *para* methoxy benzyl alcohol was used as a model substrate since similar Ru complexes have been reported to catalyze the oxidation of such derivatives.[23-27] The linear sweep voltammetry (LSV) measurements under chopped light illumination are presented in Figure 5. Pictures of the TiO_2 electrodes coated with the dyad **HOOC-(Zn)DMP-tpy-Ru** and of the experimental setup used to recorded the linear sweep voltammetry measurements are given in Figures S46 in ESI.

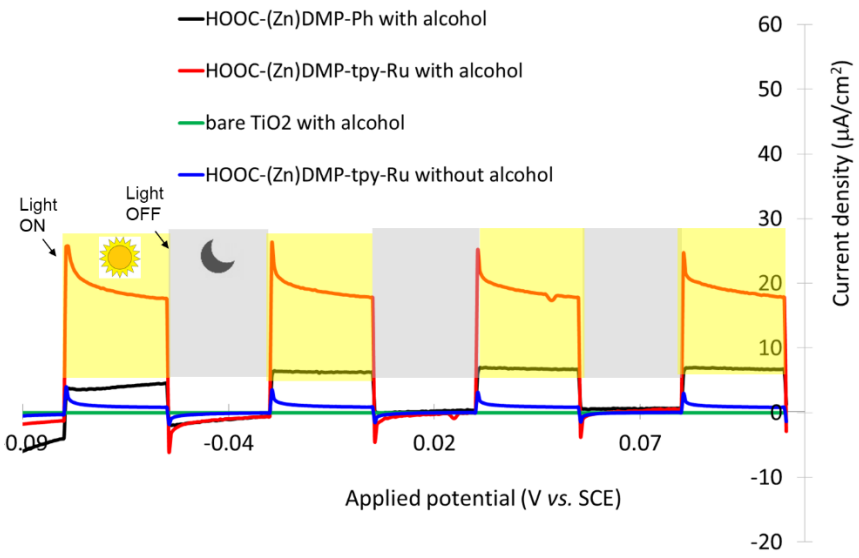

Figure 5. Linear sweep voltammetry measurements on TiO_2 photoanodes under chopped light illumination in 20 mM acetate buffer (pH = 4.75) with 0.1 M of $LiClO_4$. Scan rate 10 mV/sec. Alcohol = methoxy benzyl alcohol at the concentration of 80 mM.

As expected, the bare TiO_2 electrode does not exhibit noticeable current upon light excitation even in the presence of the alcohol substrate in the solution. The electrode sensitized with reference zinc porphyrin (**HOOC-(Zn)DMP-Ph**) exhibits some photomodulated current, but the intensity is much lower in comparison with the **HOOC-(Zn)DMP-tpy-Ru** dyad. The TiO_2 photanode coated with **HOOC-(Zn)DMP-tpy-Ru** produces a very low photocurrent in the absence of methoxy benzyl alcohol, since the photogenerated holes on the system cannot be scavenged by any substance in the solution. However, a significant photocurrent density appeared once the methoxy benzyl alcohol was introduced in the solution suggesting that the desired catalytic oxidation has taken place. The same experiment, was also conducted with the **HOOC-DMP-tpy-Ru** dyad, but the current density was even lower than with **HOOC-(Zn)DMP-tpy-Ru** (Figure S47). The free base porphyrin is more difficult to be oxidized than the zinc porphyrin, therefore the hole shift reaction to the Ru catalyst is an energetically more favorable process. However, the overall efficiency of the DSPEC sensitized with **HOOC-DMP-tpy-Ru** is certainly limited by the very inefficient electron injection reaction into TiO_2 from the photoexcited free base porphyrin, which controlled then the formation of the oxidized Ru catalyst (see PV measurements in Table 3). Using another n-type semiconductor with a lower lying conduction band such as SnO_2 could improve the quantum yield of the electron injection reaction and could lead to higher photocatalytic activity in DSPEC. Our attempt to measure the quantity of aldehyde that was produced, however, was unsuccessful due to the low current density delivered by the cell and therefore the low amount of aldehyde in the electrolyte.

Furthermore, several tpy-Ru complexes have proven to be active catalysts towards CO_2 reduction,[28-32] therefore NiO photocathodes, coated with the **HOOC-(Zn)DMP-tpy-Ru** dyad, were used as working electrodes for the fabrication of DSPECs. The reaction medium was a mixture of acetonitrile/water in a 9/1 ratio with Bu_4NPF_6 as supporting electrolyte. The NiO photocathodes were studied by LSV with chopped light irradiation after purging the solution with argon and then with CO_2 (Figure 6). The bare NiO electrode as well as that coated with **HOOC-(Zn)DMP-Ph**, lacking the Ru catalyst, give almost no photocurrent (maximum

amplitude of about 2 μA/cm^2), while under the same conditions the **HOOC-(Zn)DMP-tpy-Ru** dyad displayed significant photocurrent density (50 μA/cm^2 at -0.3 V *vs.* SCE applied potential). The amplitude of the photocurrent delivered by **HOOC-(Zn)DMP-tpy-Ru** is importantly reduced after purging the solution with argon (15 μA/cm^2 at -0.3 V *vs.* SCE applied potential), showing that the presence of CO_2 in the solution is essential for large photocurrent density to be observed.

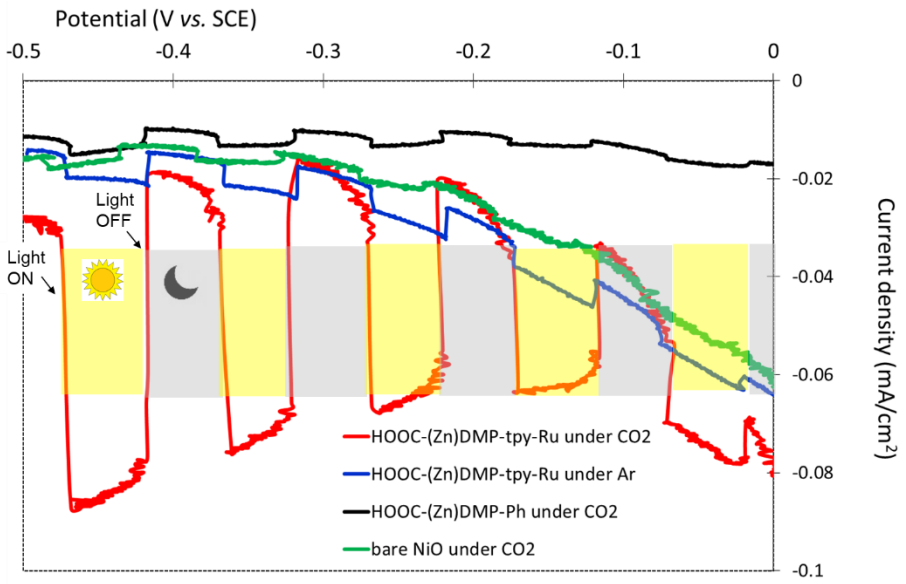

Figure 6. Linear sweep voltammetry measurements of the NiO photocathodes under chopped light illumination in acetonitrile/water (9/1) with 0.1 M of Bu_4NPF_6. Scan rate 10 mV/sec.

The photocurrent densities of the p-DSSCs sensitized by **HOOC-(Zn)DMP-Ph** and **HOOC-(Zn)DMP-tpy-Ru** differ only slightly (about 30%), while in the corresponding DSPECs the variation is much greater (about 250%), indicating that a new process takes place. CO_2 dissolved in the solution can be used as a substrate to regenerate the reduced system only in the case of the **HOOC-(Zn)DMP-tpy-Ru** dyad, while with **HOOC-(Zn)DMP-Ph** the electron on the porphyrin can only recombine with the holes in NiO valence band. Based on the results of previously reported studies, CO_2 is most probably reduced into CO or a mixture or CO+H_2 in the presence of analogues Ru complexes. Once again, we were not able to determine the photogenerated products during these experiments, owing to the low amounts that were produced.

Altogether, these experiments in DSPECs underline that the presence of the Ru complex is fundamental to observe significant current photomodulations of each substrate (benzyl alcohol in case of TiO_2 photoanode and CO_2 in the case of NiO photocathode) and they are consistent with the occurrence of a catalytic reaction initiating from tpy-Ru.

Conclusion

Four dyads composed of a porphyrin derivative (free base or metallated by zinc) connected to a ruthenium complex ($Ru(bpy)_3$ or tpy-Ru) were investigated as sensitizers in DSSCs and in DSPECs using both a n-type (TiO_2) and p-type (NiO) semiconductors. The photovoltaic measurements of the TiO_2-based DSSCs revealed that the presence of the ruthenium complex decreases the overall performances of the dyads compared to those of the parent reference

porphyrins. Conversely, in the case of NiO based p-DSSC the ruthenium complex has a positive impact, since higher values of the photovoltaic parameters were recorded for the dyads compared to those of the reference sensitizers. In DSSCs, the ruthenium complex improves the light harvesting efficiency and the most efficient dyad is **HOOC-(Zn)DMP-tpy-Ru** with both SCs. In a second step, the dyad **HOOC-(Zn)DMP-tpy-Ru** was used to fabricate DSPECs, first to oxidize methoxy-benzyl alcohol on TiO_2 photoanodes and to reduce CO_2 on NiO photocathodes. On both semiconductors, the LSV experiments demonstrate that this dyad clearly exhibits higher photocurrent density when the electrolyte contains a substrate that can be consumed by the Ru catalyst (alcohol for TiO_2 photoanode and CO_2 for NiO photocathode). On TiO_2, the efficiency could be improved by using another n-SC with more accessible CB potential such as SnO_2 to enhance the electron injection driving force from the triplet excited state of the porphyrin sensitizer. On NiO, a sensitizer exhibiting a more negative potential would give a larger driving force of the electron shift reaction and would probably increase the overall photocatalytic efficiency of the system. Utilization of better performing catalysts for CO_2 reduction (higher TOF and a lower overpotential) would be another option to increase the photocatalytic performance of the p-DSPECs. The study of two different types of photoelectrochemical devices (DSSC and DSPEC) offers the possibility to determine the optimum conditions to fabricate the photoelectrodes and to select the most promising systems to develop DSPECs. For example, the initial fabrication of DSSCs enables us to determine the best dyeing conditions (solvent composition and duration), to verify whether the assembly can sensitize the SC and to indirectly examine if the charge transfer reaction from the dye to the catalyst is effective (impact on V_{OC} and J_{SC}). Indeed, the first step in DSPECs is the charge injection from the photoexcited dye into the SC, therefore the dyad must give substantial photovoltaic performance in DSSCs in order to be used as photocatalyst in DSPECs. Accordingly, this type of study can offer guidelines for the construction of new molecular dyads as well as a better understanding of their potential activity in DSPECs. Moreover, the present study can be employed as a guide for the development of better performing photocatalytic systems by identifying the weak points of each system.

Experimental part

Materials. Compounds **1**,[41] **2**,[42] **4**,[43] **CH_3OOC-DMP-tpy-Ru**,[44] **CH_3OOC-(Zn)DMP-tpy-Ru**,[44] **CH_3OOC-DMP-Ph**[44] and **CH_3OOC-(Zn)DMP-Ph**[44] were prepared following procedures already reported in the literature.

NMR Spectra. NMR spectra were recorded on Bruker AVANCE III-500 MHz and Bruker DPX-300 MHz spectrometers using solutions in deuterated solvents and the solvent peak was chosen as the internal standard.

Mass Spectra. Mass spectra were obtained on a Bruker UltrafleXtreme matrix assisted laser desorption ionization time-of-flight (MALDI-TOF) spectrometer using trans-2-[3-(4-tert-butylphenyl)-2-methyl-2-propenylidene] malononitrile (DCTB) as matrix.

Spectroscopy. Absorption spectra were recorded on a Shimadzu UV-1700 spectrophotometer and steady-state emission spectra were obtained using a JASCO FP-6500 fluorescence spectrophotometer.

Electrochemistry. Cyclic and square wave voltammetry experiments were carried out at room temperature using an AutoLab PGSTAT20 potentiostat. All measurements were carried out in freshly distilled and deoxygenated benzonitrile in the presence of 0.1 M of tetrabutylammonium hexafluorophosphate (Bu_4NPF_6) as the supporting electrolyte, at a scan rate of 100 mV s^{-1}. A three-electrode cell setup was used with a glassy carbon working electrode, a saturated calomel (SCE) reference electrode, and a platinum wire as a counter electrode. In all measurements the ferrocene/ferrocenium couple was at 0.55 V versus SCE under the above-mentioned conditions.

3. 4'-methyl-[2,2'-bipyridine]-4-carboxylic acid (**2**) (50 mg, 0.22 mmol) was dissolved in $SOCl_2$ (3 mL) and stirred under an argon atmosphere at 80 °C for 2 h. $SOCl_2$ was then removed under reduced pressure and the resulting acyl chloride intermediate was dried under high vacuum at 50 °C for 1 h. The dry residue was dissolved in anhydrous THF (8 mL) and porphyrin **1** (80 mg, 0.11 mmol) and anhydrous triethylamine (0.1 mL) were added. The reaction mixture was heated at 70 °C overnight, under argon atmosphere. The solvents were evaporated under reduced pressure, CH_2Cl_2 (60 mL) was added and the mixture was washed with water (3 x 50 mL). The organic layer was dried with Na_2SO_4, filtered and concentrated. The desired compound was purified by column chromatography (silica gel, CH_2Cl_2/EtOH, 98:2) yielding 79 mg of **3** (yield: 74%). ^{1}H NMR (500 MHz, $CDCl_3$): δ 9.02 (s, 1H), 8.96 (m, 2H), 8.88 (d, *J* = 4.6 Hz, 2H), 8.75 (m, 6H), 8.63 (d, *J* = 4.8 Hz, 1H), 8.44 (d, *J* = 8.3 Hz, 2H), 8.40 (s, 1H), 8.33 (d, *J* = 8.3 Hz, 2H), 8.28 (d, *J* = 8.3 Hz, 2H), 8.17 (d, *J* = 8.1 Hz, 2H), 8.06 (d, *J* = 3.9 Hz, 1H), 7.30 (s, 4H), 7.28 (d, *J* = 4.6 Hz, 1H), 4.12 (s, 3H), 2.64 (s, 6H), 2.53 (s, 3H), 1.86 (s, 12H), -2.59 (s, 2H). ^{13}C NMR (125 MHz, $CDCl_3$): 167.5, 164.1, 156.3, 154.6, 150.8, 150.3, 148.2, 147.1, 143.3, 139.5, 138.8, 138.5, 138.0, 137.6, 135.3, 134.7, 130.4, 129.6, 128.0, 127.9, 125.8, 123.0, 122.7, 119.1, 118.81, 118.76, 118.04, 117.95, 52.6, 21.8, 21.6. MALDI-TOF: calcd for $C_{64}H_{53}N_7O_3$ $[M]^+$ 967.4210, found 967.4219.

CH_3OOC-DMP-Ru(bpy)$_3$. The ruthenium complex **4** (70 mg, 0.07 mmol) was added to a solution of derivative **3** (70 mg, 0.07 mmol) in acetic acid (30 mL) and the mixture was left stirring at 100 °C overnight, under nitrogen. The resulting solution was evaporated to dryness under vacuum. The crude residue was purified by column chromatography (silica gel, CH_2Cl_2/MeOH, 95:5) to obtain 92 mg of the desired product (**CH_3OOC-DMP-Ru(bpy)$_3$**) (yield: 84%). ^{1}H NMR (500 MHz, $CDCl_3$): δ 11.33 (s, 1H), 9.33 (s, 1H), 8.80 (d, *J* = 4.3 Hz, 2H), 8.72 (d, *J* = 4.6 Hz, 2H), 8.67 (d, *J* = 4.6 Hz, 2H), 8.65 (d, *J* = 4.5 Hz, 2H), 8.61 (s, 1H), 8.40 (m, 6H), 8.28 (m, 4H), 8.08 (d, *J* = 7.9 Hz, 2H), 8.03 (s br, 1H), 7.80 (m, 6H), 7.69 (m, 3H), 7.53 (m, 1H), 7.35 (m, 4H), 7.22 (s, 4H), 7.13 (m, 1H), 4.09 (s, 3H), 2.55 (s, 6H), 2.42 (s, 3H), 1.78 (s, 12H), -2.63 (s, 2H). ^{13}C NMR (125 MHz, $CDCl_3$): 167.5, 163.1, 157.8, 156.9, 156.8, 156.7, 156.5, 156.1, 151.4, 151.1, 150.6, 146.9, 144.2, 139.4, 138.4, 138.2, 138.0, 135.1, 134.6, 130.3, 129.6, 129.3, 128.0, 127.9, 126.1, 124.6, 122.4, 119.5, 119.3, 118.7, 118.0, 52.5, 21.7, 21.6, 21.4. MALDI-TOF: calcd for $C_{84}H_{68}N_{11}O_3Ru$ $[M-H]^+$ 1380.4550, found 1380.4562.

CH_3OOC-(Zn)DMP-Ru(bpy)$_3$. To a solution of **CH_3OOC-DMP-Ru(bpy)$_3$** (50 mg, 0.036 mmol) in 15 mL of CH_2Cl_2, a solution of $(CH_3COO)_2Zn{\cdot}2H_2O$ (154 mg, 0.702 mmol) in 4 mL of MeOH was added. The reaction mixture was stirred at room temperature for 24 h. After the volatiles were distilled off under vacuum, the resulting residue was purified through a column chromatography (silica gel, CH_2Cl_2/MeOH, 93:7) to collect 41 mg of **CH_3OOC-(Zn)DMP-Ru(bpy)$_3$** (yield: 78%). ^{1}H NMR (500 MHz, (DMSO-d_6)): δ 11.35 (s, 1H), 9.45 (s, 1H), 9.06 (s br, 1H), 8.90 (s br, 4H), 8.76 (d, *J* = 3.4 Hz, 2H), 8.70 (d, *J* = 4.3 Hz, 2H), 8.60 (s, 4H), 8.36 (m, 4H), 8.23 (m, 8H), 8.02 (d, *J* = 10.2 Hz, 2H), 7.89 (s, 1H), 7.80 (m, 3H), 7.61 (m, 5H), 7.47 (s br, 1H),

7.32 (s, 4H), 4.04 (s, 3H), 2.58 (s, 6H), 2.51 (s, 3H), 1.78 (s, 12H). ^{13}C NMR (125 MHz, DMSO-d_6): 166.2, 162.7, 157.1, 156.3, 156.1, 156.0, 155.4, 151.6, 150.9, 150.1, 149.7, 148.9, 148.7, 148.6, 148.3, 147.3, 142.7, 138.7, 138.4, 138.0, 137.7, 137.5, 136.5, 134.1, 131.6, 131.3, 131.0, 130.1, 129.8, 128.7, 128.2, 128.0, 127.6, 127.2, 127.0, 125.3, 124.2, 121.9, 119.1, 118.1, 117.9, 117.7, 52.0, 21.0, 20.7, 20.4. MALDI-TOF: calcd for $C_{84}H_{67}N_{11}O_3RuZn$ $[M]^+$ 1443.3763, found 1443.3771.

HOOC-DMP-Ru(bpy)$_3$. **CH$_3$OOC-DMP-Ru(bpy)$_3$** (30 mg, 0.021 mmol) was dissolved in 14 mL of a THF/MeOH mixture (2 : 1), followed by the addition of an aqueous solution (5 mL) of KOH (300 mg, 5.36 mmol) and the reaction was left under stirring at room temperature overnight. The organic solvents were evaporated under reduced pressure, and then a solution of 1 M HCl (aq) was added dropwise for the acidification of the mixture and the precipitation of the desired product. Finally, after the dyad was filtered, washed with H_2O and dried under vacuum 21 mg of **HOOC-DMP-Ru(bpy)$_3$** were isolated (yield: 73%). ^{1}H NMR (500 MHz, (DMSO-d_6)): δ 12.57 (s, 1H), 9.80 (s,1H), 9.07 (s, 1H), 8.82 (m, 8H), 8.61 (d, J = 16.7 Hz, 4H), 8.23 (m, 13H), 7.99 (s, 1H0, 7.91 (s, 1H), 7.80 (m, 3H), 7.60 (m, 5H), 7.42 (s, 1H), 7.30 (s, 4H), 2.63 (s, 6H), 2.37 (s, 3H), 1.72 (s, 12H), -2.74 (s, 2H) ppm. A ^{13}C NMR spectrum could not be obtained due to the low solubility of this compound. MALDI-TOF: calcd for $C_{83}H_{66}N_{11}O_3Ru$ $[M-H]^+$ 1366.4394, found 1366.4388. UV–Vis in THF/MeOH [λmax/nm (ε/mM^{-1} cm^{-1})]: 294 (60.2), 418 (409.3), 514 (22.4), 549 (11.8), 591 (6.2), 649 (5.0).

HOOC-(Zn)DMP-Ru(bpy)$_3$. **CH$_3$OOC-(Zn)DMP-Ru(bpy)$_3$** (25 mg, 0.017 mmol) was dissolved in 10 mL of a THF/MeOH mixture (2 : 1), followed by the addition of an aqueous solution (4 mL) of KOH (150 mg, 2.68 mmol) and the reaction was left under stirring at room temperature overnight. The organic solvents were evaporated under reduced pressure, and then a solution of 1 M HCl (aq) was added dropwise for the acidification of the mixture and the precipitation of the desired product. Finally, after the dyad was filtered, washed with H_2O and dried under vacuum 21 mg of **HOOC-(Zn)DMP-Ru(bpy)$_3$** were isolated (yield: 85%). ^{1}H NMR and ^{13}C NMR spectra could not be recorded due to solubility reasons. MALDI-TOF: calcd for $C_{83}H_{65}N_{11}O_3RuZn$ $[M]^+$ 1429.3607, found 1429.3616. UV–Vis in THF/MeOH [λmax/nm (ε/mM^{-1} cm^{-1})]: 286 (131.2), 425 (563.7), 468 (24.2), 558 (28.7), 598 (12.7).

HOOC-DMP-tpy-Ru. **CH$_3$OOC-DMP-tpy-Ru** (25 mg, 0.018 mmol) was dissolved in 10 mL of a THF/MeOH mixture (2 : 1), followed by the addition of an aqueous solution (4 mL) of KOH (100 mg, 1.79 mmol) and the reaction was left under stirring at room temperature overnight. The organic solvents were evaporated under reduced pressure, and then a solution of 1 M HCl (aq) was added dropwise for the acidification of the mixture and the precipitation of the desired product. Finally, after the dyad was filtered, washed with H_2O and dried under vacuum 26 mg of **HOOC-DMP-tpy-Ru** were isolated (yield: 96%). ^{1}H NMR (500 MHz, (DMSO-d_6)): δ 10.92 (s, 1H), 10.12 (d, J = 4.8 Hz, 1H), 9.29 (s, 2H), 8.97 (d, J = 8.0 Hz, 2H), 8.90 (m, 3H), 8.80 (d, J = 4.3 Hz, 2H), 8.65 (m, 4H), 8.58 (d, J = 7.9 Hz, 2H), 8.43 (d, J = 8.0 Hz, 2H), 8.33 (m, 8H), 8.26 (m, 2H), 8.06 (m, 3H), 7.79 (t, J = 7.4 Hz, 1H), 7.67 (d, J = 5.7 Hz, 2H), 7.46 (d, J = 5.8 Hz, 1H), 7.42 (t, J = 6.4 Hz, 2H), 7.35 (s, 4H), 7.10 (t, J = 6.3 Hz, 1H), 2.58 (s, 6H), 1.77 (s, 12H), -2.73 (s, 2H) ppm. ^{13}C NMR (125 MHz, (DMSO-d_6)): 167.7, 165.6, 158.7, 158.4, 158.2, 155.7, 152.1, 152.0, 151.9, 145.6, 144.1, 139.6, 139.2, 138.6, 137.9, 137.8, 137.3, 136.9, 136.5, 136.0, 135.9, 134.8, 134.6, 130.5, 129.0, 128.0, 127.8, 127.1, 126.6, 124.3, 123.9, 123.7, 120.3, 119.7, 119.1, 118.3, 118.1, 21.3, 21.2. MALDI-TOF: calcd for $C_{83}H_{64}Cl_2N_{10}O_3Ru$ $[M-Cl]^+$ 1385.3895, found 1385.3883. UV–Vis in THF [λmax/nm (ε/mM^{-1} cm^{-1})]: 292 (55.9), 324 (33.8), 421 (355.3), 516 (25.3), 550 (14.0), 590 (4.1), 647 (1.4).

HOOC-(Zn)DMP-tpy-Ru. **CH_3OOC-(Zn)DMP-tpy-Ru** (25 mg, 0.017 mmol) was dissolved in 10 mL of a THF/MeOH mixture (2 : 1), followed by the addition of an aqueous solution (4 mL) of KOH (480 mg, 5.56 mmol) and the reaction was left under stirring at room temperature overnight. The organic solvents were evaporated under reduced pressure, and then a solution of 1 M HCl (aq) was added dropwise for the acidification of the mixture and the precipitation of the desired product. Finally, after the dyad was filtered, washed with H_2O and dried under vacuum 25 mg of **HOOC-(Zn)DMP-tpy-Ru** were isolated (yield: 98%). ^{1}H NMR (500 MHz, (DMSO-d_6)): *δ* 13.10 (s br, 1H), 10.88 (s, 1H), 10.14 (d, *J* = 5.1 Hz, 1H), 9.34 (s, 2H), 9.02 (d, *J* = 8.1 Hz, 2H), 8.95 (d, *J* = 8.2 Hz, 1H), 8.83 (d, *J* = 4.5 Hz, 2H), 8.72 (d, *J* = 4.6 Hz, 2H), 8.67 (d, *J* = 8.3 Hz, 1H), 8.61 (m, 6H), 8.45 (d, *J* = 8.2 Hz, 2H), 8.39 (t, *J* = 7.8 Hz, 1H), 8.32 (m, 6H), 8.23 (d, *J* = 8.4 Hz, 2H), 8.09 (m, 3H), 7.81 (t, *J* = 7.3 Hz, 1H), 7.68 (d, J = 5.7 Hz, 2H), 7.49 (d, J = 5.9 Hz, 1H), 7.44 (t, *J* = 6.4 Hz, 2H), 7.33 (s, 4H), 7.11 (t, *J* = 6.5 Hz, 1H), 2.59 (s, 6H), 1.80 (s, 12H) ppm. ^{13}C NMR (125 MHz, DMSO-d_6): 167.6, 165.3, 158.6, 158.3, 158.0, 155.6, 152.0, 151.9, 149.4, 149.1, 149.0, 148.7, 147.3, 143.8, 139.3, 139.1, 138.6, 138.4, 138.1, 137.1, 136.9, 136.1, 135.7, 134.5, 134.4, 132.1, 131.7, 130.4, 130.1, 129.8, 128.8, 127.6, 127.5, 127.0, 126.5, 124.2, 123.8, 123.5, 120.2, 119.7, 118.5, 118.2, 21.4, 21.1. MALDI-TOF: calcd for $C_{83}H_{62}ClN_{10}O_3RuZn$ $[M]^+$ 1447.3030, found 1447.3041. UV–Vis in THF [λmax/nm (ε/mM^{-1} cm^{-1})]: 295 (52.6), 325 (35.5), 431 (494.2), 518 (13.6), 561 (24.2), 604 (7.8).

HOOC-DMP-Ph. To a solution of **CH_3OOC-DMP-Ph** (25 mg, 0.027 mmol) was dissolved in 15 mL of a THF/MeOH mixture (2 : 1), an aqueous solution (6 mL) of KOH (380 mg, 6.80 mmol) was added and the reaction was left under stirring at room temperature overnight. The organic solvents were evaporated under reduced pressure, and then a solution of 1 M HCl (aq) was added dropwise for the acidification of the mixture and the precipitation of the desired product. Finally, after the dyad was filtered, washed with H_2O and dried under vacuum 22 mg of **HOOC-DMP-Ph** were isolated (yield: 77%). ^{1}H NMR (500 MHz, (DMSO-d_6)): *δ* 10.70 (s, 1H), 8.89 (d, *J* = 4.4 Hz, 2H), 8.79 (d, *J* = 4.4 Hz, 2H), 8.65 (m, , *J* = 4.4 Hz, 4H), 8.35 (s, 4H), 8.26 (d, *J* = 8.6 Hz, 2H), 8.22 (d, *J* = 8.6 Hz, 2H), 8.11 (d, *J* = 6.8 Hz, 2H), 7.64 (m, 3H), 7.34 (s, 4H), 2.57 (s, 6H), 1.76 (s, 12H), -2.73 (s, 2H) ppm. ^{13}C NMR (125 MHz, (DMSO-d_6)): 167.5, 166.1, 145.5, 139.3, 138.4, 137.6, 136.0, 135.2, 134.6, 134.4, 131.7, 130.4, 128.5, 127.9, 127.8, 119.7, 118.6, 118.0, 117.9, 21.2, 21.0. MALDI-TOF: calcd for $C_{58}H_{47}N_5O_3$ $[M]^+$ 861.3679, found 861.3687. UV–Vis in THF [λmax/nm (ε/mM^{-1} cm^{-1})]: 419 (368.0), 513 (13.6), 548 (6.4), 594 (3.2), 648 (4.0).

HOOC-(Zn)DMP-Ph. To a solution of **CH_3OOC-(Zn)DMP-Ph** (25 mg, 0.027 mmol) in 10 mL of a THF/MeOH mixture (2 : 1), an aqueous solution (4 mL) of KOH (190 mg, 3.39 mmol) was added and the reaction was left under stirring at room temperature overnight. The organic solvents were evaporated under reduced pressure, and then a solution of 1 M HCl (aq) was added dropwise for the acidification of the mixture and the precipitation of the desired product. Finally, after the dyad was filtered, washed with H_2O and dried under vacuum 23 mg of **HOOC-(Zn)DMP-Ph** were isolated (yield: 92%). ^{1}H NMR (500 MHz, (DMSO-d_6)): *δ* 10.67 (s, 1H), 8.80 (d, *J* = 4.5 Hz, 2H), 8.72 (d, *J* = 4.4 Hz, 2H), 8.58 (d, *J* = 4.4 Hz, 4H), 8.33 (m, 2H), 8.26 (d, *J* = 7.7 Hz, 2H), 8.21 (d, *J* = 8.5 Hz, 2H), 8.17 (d, *J* = 8.5 Hz, 2H), 8.12 (d, *J* = 6.9 Hz, 2H), 7.64 (m, 3H), 7.31 (s, 4H), 2.58 (s, 6H), 1.78 (s, 12H) ppm. ^{13}C NMR (125 MHz, DMSO-d_6): 166.0, 149.4, 149.1, 149.0, 148.9, 145.7, 139.2, 138.7, 138.4, 137.9, 135.2, 134.4, 134.1, 132.1, 131.8, 131.7, 130.2, 130.1, 128.5, 127.8, 127.6, 127.4, 119.6, 118.7, 118.3, 118.1, 21.4, 21.1. MALDI-TOF: calcd for $C_{58}H_{45}N_5O_3Zn$ $[M]^+$ 923.2814, found 923.2805. UV–Vis in THF [λmax/nm (ε/mM^{-1} cm^{-1})]: 426 (452.3), 555 (16.6), 598 (5.7).

Acknowledgements

This research was funded by the General Secretariat for Research and Technology (GSRT) and Hellenic Foundation for Research and Innovation (HFRI; project code: 508). This research has also been co-financed by the European Union and Greek national funds through the Operational Program Competitiveness, Entrepreneurship, and Innovation, under the call RESEARCH− CREATE−INNOVATE (project code: T1EDK-01504). In addition, this research has been co-financed by the European Union and Greek national funds through the Regional Operational Program "Crete 2014-2020," project code OPS:5029187. Moreover, the European Commission's Seventh Framework Program (FP7/2007-2013) under grant agreement no. 229927 (FP7-REGPOT-2008-1, Project BIO-SOLENUTI) and the Special Research Account of the University of Crete are gratefully acknowledged for the financial support of this research. Finally, this research is co-financed by Greece and the European Union (European Social Fund-ESF) through the Operational Programme «Human Resources Development, Education and Lifelong Learning 2014-2020» in the context of the project "Photocatalytic H_2 production and CO_2 reduction using self-assembled chromophore-catalyst nanostructures" (MIS 5048472).

References

[1] Hagfeldt A, Boschloo G, Sun L, Kloo L, Pettersson H. Dye-Sensitized Solar Cells. Chem. Rev. 2010; 110: 6595-663.

[2] Odobel F, Pellegrin Y. Recent advances in the sensitization of wide-band-gap nanostructured p-type semiconductors. Photovoltaic and photocatalytic applications. Journal of Physical Chemistry Letters 2013; 4: 2551-64.

[3] Ashford DL, Gish MK, Vannucci AK, Brennaman MK, Templeton JL, Papanikolas JM, Meyer TJ. Molecular Chromophore-Catalyst Assemblies for Solar Fuel Applications. Chemical Reviews (Washington, DC, United States) 2015; 115: 13006-49.

[4] Gibson EA. Dye-sensitized photocathodes for H2 evolution. Chem. Soc. Rev. 2017; 46: 6194-209.

[5] Swierk JR, Mallouk TE. Design and development of photoanodes for water-splitting dye-sensitized photoelectrochemical cells. Chem. Soc. Rev. 2013; 42: 2357-87.

[6] Brennaman MK, Dillon RJ, Alibabaei L, Gish MK, Dares CJ, Ashford DL, House RL, Meyer GJ, Papanikolas JM, Meyer TJ. Finding the Way to Solar Fuels with Dye-Sensitized Photoelectrosynthesis Cells. J. Am. Chem. Soc. 2016; 138: 13085-102.

[7] Grätzel M. Photovoltaic performance and long-term stability of dye-sensitized meosocopic solar cells. C. R. Chimie 2006; 9: 578-83.

[8] Mathew S, Yella A, Gao P, Humphry-Baker R, Curchod BFE, Ashari-Astani N, Tavernelli I, Rothlisberger U, Nazeeruddin MK, Grätzel M. Dye-sensitized solar cells with 13% efficiency achieved through the molecular engineering of porphyrin sensitizers. Nature Chem. 2014; 6: 242.

[9] Yella A, Lee H-W, Tsao HN, Yi C, Chandiran AK, Nazeeruddin MK, Diau EW-G, Yeh C-Y, Zakeeruddin SM, Grätzel M. Porphyrin-Sensitized Solar Cells with Cobalt (II/III)–Based Redox Electrolyte Exceed 12 Percent Efficiency. Science 2011; 334: 629.

[10] Zhang L, Yang X, Wang W, Gurzadyan GG, Li J, Li X, An J, Yu Z, Wang H, Cai B, Hagfeldt A, Sun L. 13.6% Efficient Organic Dye-Sensitized Solar Cells by Minimizing Energy Losses of the Excited State. ACS Energy Lett. 2019; 4: 943-51.

[11] Kakiage K, Aoyama Y, Yano T, Oya K, Fujisawa J-i, Hanaya M. Highly-efficient dye-sensitized solar cells with collaborative sensitization by silyl-anchor and carboxy-anchor dyes. Chem. Commun. 2015; 51: 15894-97.

[12] Li L-L, Diau EW-G. Porphyrin-sensitized solar cells. Chem. Soc. Rev. 2013; 42: 291-304.

[13] Urbani M, Grätzel M, Nazeeruddin MK, Torres T. Meso-Substituted Porphyrins for Dye-Sensitized Solar Cells. Chem. Rev. 2014; 114: 12330-96.
[14] Grzegorzek N, Zieleniewska A, Schür A, Maichle-Mössmer C, Killian MS, Guldi DM, Chernick ET. Electronically Tuned Asymmetric meso-Substituted Porphyrins for p-Type Solar Cells. ChemPlusChem 2019; 84: 766-71.
[15] Jianfeng L, Zonghao L, Narendra P, Liangcong J, Udo B, N. SA, Yi-Bing C, Leone S. Molecular Engineering of Zinc-Porphyrin Sensitisers for p-Type Dye-Sensitised Solar Cells. ChemPlusChem 2018; 83: 711-20.
[16] Zhang L, Favereau L, Farre Y, Maufroy A, Pellegrin Y, Blart E, Hissler M, Jacquemin D, Odobel F, Hammarstrom L. Molecular-structure control of electron transfer dynamics of push-pull porphyrins as sensitizers for NiO based dye sensitized solar cells. RSC Adv. 2016; 6: 77184-94.
[17] Maufroy A, Favereau L, Anne FB, Pellegrin Y, Blart E, Hissler M, Jacquemin D, Odobel F. Synthesis and properties of push-pull porphyrins as sensitizers for NiO based dye-sensitized solar cells. J. Mater. Chem. A 2015; 3: 3908-17.
[18] Borgström M, Blart E, Boschloo G, Mukhtar E, Hagfeldt A, Hammarström L, Odobel F. Sensitized Hole Injection of Phosphorus Porphyrin into NiO: Toward New Photovoltaic Devices. J. Phys. Chem. B 2005; 109: 22928-34.
[19] He J, Lindström H, Hagfeldt A, Lindquist S-E. Dye-Sensitized Nanostructured p-Type Nickel Oxide Film as a Photocathode for a Solar Cell. J. Phys. Chem. B 1999; 103: 8940-43.
[20] Nikolaou V, Plass F, Planchat A, Charisiadis A, Charalambidis G, Angaridis PA, Kahnt A, Odobel F, Coutsolelos AG. Effect of the triazole ring in zinc porphyrin-fullerene dyads on the charge transfer processes in NiO-based devices. Physical Chemistry Chemical Physics 2018; 20: 24477-89.
[21] Harriman A, Odobel F, Sauvage J-P. Multistep Electron Transfer in a Porphyrin-Ruthenium(II) Bis(terpyridyl)-Porphyrin Triad. J. Am. Chem. Soc. 1994; 116: 5481-82.
[22] Collin J-P, Harriman A, Heitz V, Odobel F, Sauvage J-P. Photoinduced Electron- and Energy-Transfer Processes Occurring within Porphyrin-Metal-Bisterpyridyl Conjugates. J. Am. Chem. Soc. 1994; 116: 5679-90.
[23] Song W, Vannucci AK, Farnum BH, Lapides AM, Brennaman MK, Kalanyan B, Alibabaei L, Concepcion JJ, Losego MD, Parsons GN, Meyer TJ. Visible Light Driven Benzyl Alcohol Dehydrogenation in a Dye-Sensitized Photoelectrosynthesis Cell. J. Am. Chem. Soc. 2014; 136: 9773-79.
[24] Vannucci AK, Hull JF, Chen Z, Binstead RA, Concepcion JJ, Meyer TJ. Water Oxidation Intermediates Applied to Catalysis: Benzyl Alcohol Oxidation. J. Am. Chem. Soc. 2012; 134: 3972-75.
[25] Ishizuka T, Kotani H, Kojima T. Characteristics and reactivity of ruthenium–oxo complexes. Dalton Trans. 2016; 45: 16727-50.
[26] Li F, Yu M, Jiang Y, Huang F, Li Y, Zhang B, Sun L. Chemical and photochemical oxidation of organic substrates by ruthenium aqua complexes with water as an oxygen source. Chem. Commun. 2011; 47: 8949-51.
[27] Chen W, Rein FN, Rocha RC. Homogeneous Photocatalytic Oxidation of Alcohols by a Chromophore–Catalyst Dyad of Ruthenium Complexes. Angew. Chem. Int. Ed. 2009; 48: 9672-75.
[28] Chen Z, Chen C, Weinberg DR, Kang P, Concepcion JJ, Harrison DP, Brookhart MS, Meyer TJ. Electrocatalytic reduction of CO2 to CO by polypyridyl ruthenium complexes. Chem. Commun. 2011; 47: 12607-09.
[29] Chen Z, Kang P, Zhang M-T, Meyer TJ. Making syngas electrocatalytically using a polypyridyl ruthenium catalyst. Chem. Commun. 2014; 50: 335-37.

[30] Johnson BA, Maji S, Agarwala H, White TA, Mijangos E, Ott S. Activating a Low Overpotential CO2 Reduction Mechanism by a Strategic Ligand Modification on a Ruthenium Polypyridyl Catalyst. Angew. Chem. Int. Ed. 2016; 55: 1825-29.
[31] White TA, Maji S, Ott S. Mechanistic insights into electrocatalytic CO2 reduction within [RuII(tpy)(NN)X]n+ architectures. Dalton Trans. 2014; 43: 15028-37.
[32] Li T-T, Shan B, Xu W, Meyer TJ. Electrocatalytic CO2 Reduction with a Ruthenium Catalyst in Solution and on Nanocrystalline TiO2. ChemSusChem 2019; 12: 2402-08.
[33] Wang F, Stahl SS. Electrochemical Oxidation of Organic Molecules at Lower Overpotential: Accessing Broader Functional Group Compatibility with Electron−Proton Transfer Mediators. Acc. Chem. Res. 2020; 53: 561-74.
[34] Treadway JA, Moss JA, Meyer TJ. Visible Region Photooxidation on TiO2 with a Chromophore−Catalyst Molecular Assembly. Inorg. Chem. 1999; 38: 4386-87.
[35] Windle CD, Kumagai H, Higashi M, Brisse R, Bold S, Jousselme B, Chavarot-Kerlidou M, Maeda K, Abe R, Ishitani O, Artero V. Earth-Abundant Molecular Z-Scheme Photoelectrochemical Cell for Overall Water-Splitting. J. Am. Chem. Soc. 2019; 141: 9593-602.
[36] Sahara G, Kumagai H, Maeda K, Kaeffer N, Artero V, Higashi M, Abe R, Ishitani O. Photoelectrochemical Reduction of CO2 Coupled to Water Oxidation Using a Photocathode with a Ru(II)–Re(I) Complex Photocatalyst and a CoOx/TaON Photoanode. J. Am. Chem. Soc. 2016; 138: 14152-58.
[37] Sahara G, Abe R, Higashi M, Morikawa T, Maeda K, Ueda Y, Ishitani O. Photoelectrochemical CO2 reduction using a Ru(ii)-Re(i) multinuclear metal complex on a p-type semiconducting NiO electrode. Chem. Commun. 2015; 51: 10722-25.
[38] Kou Y, Nakatani S, Sunagawa G, Tachikawa Y, Masui D, Shimada T, Takagi S, Tryk DA, Nabetani Y, Tachibana H, Inoue H. Visible light-induced reduction of carbon dioxide sensitized by a porphyrin–rhenium dyad metal complex on p-type semiconducting NiO as the reduction terminal end of an artificial photosynthetic system. J. Cata. 2014; 310: 57-66.
[39] Odobel F, Pellegrin Y, Gibson EA, Hagfeldt A, Smeigh AL, Hammarström L. Recent advances and future directions to optimize the performances of p-type dye-sensitized solar cells. Coord. Chem. Rev. 2012; 256: 2414-23.
[40] Nikolaou V, Charisiadis A, Charalambidis G, Coutsolelos AG, Odobel F. Recent advances and insights in dye-sensitized NiO photocathodes for photovoltaic devices. Journal of Materials Chemistry A 2017; 5: 21077-113.
[41] Zervaki GE, Papastamatakis E, Angaridis PA, Nikolaou V, Singh M, Kurchania R, Kitsopoulos TN, Sharma GD, Coutsolelos AG. A Propeller-Shaped, Triazine-Linked Porphyrin Triad as Efficient Sensitizer for Dye-Sensitized Solar Cells. European Journal of Inorganic Chemistry 2014; 2014: 1020-33.
[42] McCafferty DG, Bishop BM, Wall CG, Hughes SG, Mecklenberg SL, Meyer TJ, Erickson BW. Synthesis of redox derivatives of lysine and their use in solid-phase synthesis of a light-harvesting peptide. Tetrahedron 1995; 51: 1093-106.
[43] Sullivan BP, Salmon DJ, Meyer TJ. Mixed phosphine 2,2'-bipyridine complexes of ruthenium. Inorganic Chemistry 1978; 17: 3334-41.
[44] Quaranta A, Charalambidis G, Herrero C, Margiola S, Leibl W, Coutsolelos A, Aukauloo A. Synergistic “ping-pong” energy transfer for efficient light activation in a chromophore–catalyst dyad. Physical Chemistry Chemical Physics 2015; 17: 24166-72.
[45] Stangel C, Ladomenou K, Charalambidis G, Panda MK, Lazarides T, Coutsolelos AG. Synthesis, Characterization and Electronic Properties of trans-[4-(Alkoxycarbonyl)phenyl]porphyrin-[RuII(bpy)$_3$]$_2$ Complexes or Boron–Dipyrrin Conjugates as Panchromatic Sensitizers for DSSCs. European Journal of Inorganic Chemistry 2013; 2013: 1275-86.

[46] Ha-Thi MH, Pham VT, Pino T, Maslova V, Quaranta A, Lefumeux C, Leibl W, Aukauloo A. Photoinduced electron transfer in a molecular dyad by nanosecond pump–pump–probe spectroscopy. Photochem. Photobiol. Sci. 2018; 17: 903-09.
[47] Herrero C, Quaranta A, Fallahpour R-A, Leibl W, Aukauloo A. Identification of the Different Mechanisms of Activation of a [RuII(tpy)(bpy)(OH2)]2+ Catalyst by Modified Ruthenium Sensitizers in Supramolecular Complexes. J. Phys. Chem. C 2013; 117: 9605-12.
[48] Raga SR, Barea EM, Fabregat-Santiago F. Analysis of the Origin of Open Circuit Voltage in Dye Solar Cells. Journal of Physical Chemistry Letters 2012; 3: 1629-34.
[49] Bai Y, Zhang J, Wang Y, Zhang M, Wang P. Lithium-Modulated Conduction Band Edge Shifts and Charge-Transfer Dynamics in Dye-Sensitized Solar Cells Based on a Dicyanamide Ionic Liquid. Langmuir 2011; 27: 4749-55.
[50] Carella A, Borbone F, Centore R. Research Progress on Photosensitizers for DSSC. Frontiers in Chemistry 2018; 6.
[51] Bonhôte P, Moser J-E, Humphry-Baker R, Vlachopoulos N, Zakeeruddin SM, Walder L, Grätzel M. Long-Lived Photoinduced Charge Separation and Redox-Type Photochromism on Mesoporous Oxide Films Sensitized by Molecular Dyads. J. Am. Chem. Soc. 1999; 121: 1324-36.